Anomalous elastic properties of superionic ice

Shichuan Sun,[1,2] Yu He,[1,3,*] Duck Young Kim,[3] and Heping Li[1,*]

[1]*Key Laboratory of High-Temperature and High-Pressure Study of the Earth's Interior, Institute of Geochemistry, Chinese Academy of Sciences, Guiyang, Guizhou 550081, China*

[2]*University of Chinese Academy of Sciences, Beijing 100049, China*

[3]*Center for High Pressure Science and Technology Advanced Research, Shanghai 201203, China*

(Received 15 October 2019; revised 20 August 2020; accepted 25 August 2020; published 21 September 2020)

Elastic properties and sound velocities of superionic ice X and ice XVIII are investigated using *ab initio* molecular dynamics at 200 GPa and temperatures up to 4500 K. The dislocation of protons from their lattice sites leads to the significant elastic softening in ice X with increasing temperature. The phase transition from ice X to ice XVIII leads to an increasing in proton diffusion and elastic softening at 2000 K. We also observed the elastic stiffening with increasing temperature from 2000 to 3000 K in ice XVIII, which is similar to the behavior of some liquids. Above 3000 K, all the elastic constants decrease dramatically. Our study suggests proton diffusion has significant influence on the elastic properties, and the elastic property of superionic ice with increasing temperature is different from ordinary solids.

DOI: 10.1103/PhysRevB.102.104108

I. INTRODUCTION

H_2O shows an intricate phase diagram under high pressure and temperature (P-T) [1,2]. The normal asymmetric hydroxyl O-H bond at low pressure transforms to symmetric O-H-O bond in ice X at high pressure [3–5]. Further increasing temperature leads to the fast diffusion of protons in the oxygen sublattice and forms the superionic phase [6–18]. Superionic (SI) ice is an exotic state, which was predicted by DFT calculations [6–13] and then confirmed by high pressure experiments [14–18]. Within SI ice, hydrogen is no longer bonded to oxygen, and diffuses like liquid, whereas the oxygen atoms are still fixed at their sites forming a solid sublattice, which enables SI ice to have both solid and liquid behaviors. SI ice has a high melting temperature with a wide stability field, and can exist in the interiors of Uranus and Neptune, which could make it a prevalent H_2O phase in our solar system. Recent shock compression experiments reported phase transitions from solid ice X to SI ice XVIII when temperature was increased to over 2000 K at pressures greater than 100 GPa [18]. The ice X to ice XVIII phase transition, which leads to a structural change in the oxygen sublattice from body-centered-cubic (bcc) to face-centered-cubic (fcc), is ascribed to the contribution of extra entropy associated with the fluidlike protons [18]. In addition, the highly diffusive protons leads to high ionic conductivity of over 10^4 S m^{-1}, and it has been suggested to influence the nondipolar magnetic fields of Uranus and Neptune [7,17–20].

To understand the phase transition behavior of ice under pressure, it is essential to study its elastic properties. Such knowledge is crucial when modeling the structure and convection in interiors of ice giant exoplanets. Both the elastic properties and sound velocities of ice VII and ice X do not show discontinuous changes in Brillouin scattering measurements up to 100 GPa [21], whereas DFT studies show an obvious elastic shifting at ∼100–110 GPa ascribing to hydrogen bond symmetrization [22,23]. Increasing the pressure from 100 to 350 GPa is also required to the change of elasticity and dislocation behavior of ice X [24]. Hernandez and Caracas identified the ice VII" phase by observing a dip in the elastic constants along with a shrinking of the O-O distance under pressure [12]. These studies mainly focus on the changes in ice elasticity with increasing pressure, and find hydrogen symmetrization leads to significant influence on the elastic property. However, there is very little study concerning elasticity change during the solid-superionic in ice X and ice X to ice XVIII phase transitions with increasing temperature. In SI ice, liquid-like protons continually change their position in the lattice, which may significantly influence the elastic properties of SI ice. Investigation changes in the elastic property of ice with respect to temperature is essential for understanding the interiors of ice giant exoplanets. In addition, superionic materials are widely used in energy storage devices [25]. Our study may also provide insights on the elasticity of these materials.

II. COMPUTATIONAL DETAILS

A. Proton Diffusion coefficient calculations

Ab initio calculations were based on the DFT [26,27]. We used *ab initio* molecular dynamics (AIMD) to study the influence of highly diffusive protons on the elastic properties [28–30]. The Vienna *ab initio* simulation package (VASP) was employed for AIMD calculations [31]. We used the Perdew-Burke-Ernzerhof exchange-correlation functional and

*Corresponding Authors: heyu@mail.gyig.ac.cn; liheping@mail.gyig.ac.cn

projector augmented wave pseudopotentials in the calculations [32] with an energy cutoff of 400 eV. Brillouin zone sampling was performed at the Γ point. The supercells for AIMD simulations of ice X and ice XVIII contain 162 and 324 atoms, respectively.

To study proton diffusion property in SI ice, we have calculated the diffusion coefficient by the mean square displacement (MSD) of the ionic positions. The diffusion coefficient is defined as

$$D = \lim_{0\to\infty}\left[\frac{1}{2dt}[\vec{r}(t)]^2\right], \tag{1}$$

where d is the dimension of the lattice on which ion hopping takes place. The MSD

$$\langle[\vec{r}(t)]^2\rangle = \frac{1}{N}\sum_{i=1}^{N}\langle[\overrightarrow{r_i}(t+t_0) - \overrightarrow{r_i}(t_0)]^2\rangle \tag{2}$$

is averaged over all protons, and $\overrightarrow{r_i}(t)$ is the displacement of the ith proton at time t, and N is the total number of protons in the system.

The proton conductivities are calculated based on the diffusion coefficients and the Nernst-Einstein equation:

$$\sigma = \frac{fDcq^2}{kT}, \tag{3}$$

where σ is the proton conductivity, f is a numerical factor approximately equal to unity, D is the diffusion coefficient, c is the concentration of protons, q is the electrical charge of a proton, k is the Boltzmann constant, and T is the temperature.

B. Elastic constants and sound velocities calculations

The elastic properties of crystal are expressed as the relationship between stress and strain:

$$\sigma_{ij} = C_{ijkl}\varepsilon_{kl}, \tag{4}$$

where σ_{ij} refers to the stress tensor, ε_{kl} refers to the strain tensor, and C_{ijkl} represents the fourth-order elastic modulus. Considering of the symmetry of C_{ijkl}, the equation is simplified as below:

$$\sigma_i = C_{ij}\varepsilon_j. \tag{5}$$

The equation could be expanded as follows:

$$\begin{pmatrix}\sigma_1\\ \sigma_2\\ \sigma_3\\ \sigma_4\\ \sigma_5\\ \sigma_6\end{pmatrix} = \begin{pmatrix}C_{11} & C_{12} & C_{13} & C_{14} & C_{15} & C_{16}\\ & C_{22} & C_{23} & C_{24} & C_{25} & C_{26}\\ & & C_{33} & C_{34} & C_{35} & C_{36}\\ & & & C_{44} & C_{45} & C_{46}\\ & & & & C_{55} & C_{56}\\ & & & & & C_{66}\end{pmatrix}\cdot\begin{pmatrix}\varepsilon_1\\ \varepsilon_2\\ \varepsilon_3\\ \varepsilon_4\\ \varepsilon_5\\ \varepsilon_6\end{pmatrix}. \tag{6}$$

For the cubic system investigated in this work, we have calculated the three nonequivalent elastic constants, C_{11}, C_{12}, and C_{44}. C_{11}, C_{12} could be obtained by a strain tensor:

$$\varepsilon = \begin{pmatrix}\delta & 0 & 0\\ 0 & 0 & 0\\ 0 & 0 & 0\end{pmatrix}, \tag{7}$$

and we obtained C_{44} using a strain tensor:

$$\varepsilon = \begin{pmatrix}0 & 0 & 0\\ 0 & 0 & \delta/2\\ 0 & \delta/2 & 0\end{pmatrix}, \tag{8}$$

where δ is the magnitude of distortion. For δ in ±0.01, ±0.005 and 0, five groups of strains were added by

$$a' = a(\mathrm{I} + \varepsilon), \tag{9}$$

where a represents a 3×3 cell parameter matrix, and ε represents added strain $\Delta\varepsilon$, and I represents a 3×3 identity matrix. Then, we obtained an elastic moduli trough dealing with the stress-strain relationship listed in Eq. (5). In order to ensure the reliability and full convergence of the results, 10 000 time steps of NVT simulations were carried out for each direction of deformation. The final results of the strain-stress data show a very good linear relationship and were fitted to Eq. (6) employing central difference method. For each optimizing result, the calculated correlation coefficient R^2 were larger than 99%. The calculated C_{ij} results satisfy with Born's stability conditions:

$$C_{11} - C_{12} > 0,\ C_{11} + 2C_{12} > 0,\ C_{44} > 0. \tag{10}$$

Employing the Voigt-Ruess-Hill scheme [33], we evaluated the bulk modulus (B) and shear modulus (G) and further calculated the primary wave velocity (V_P), shear wave velocity (V_S), and bulk sound velocity ($V_\emptyset$):

$$V_P = \sqrt{\frac{B + \frac{4G}{3}}{\rho}},\quad V_S = \sqrt{\frac{G}{\rho}},\quad V_\emptyset = \sqrt{\frac{B}{\rho}}. \tag{11}$$

We qualified the degree of elastic anisotropy of ice X and ice XVIII with the Zener ratio [34]:

$$\mathrm{A} = \frac{2C_{44}}{C_{11} - C_{12}}. \tag{12}$$

To further investigate the elastic anisotropy, the three-dimensional (3D) directional dependence of elastic modulus is studied using the following relation:

$$\frac{1}{\boldsymbol{E_\omega}} = \left(1 - l_3^2\right)^2 s_{11} + l_3^4 s_{33} + l_3^2\left(1 - l_3^2\right)(2s_{13} + s_{44}), \tag{13}$$

where $\boldsymbol{E_\omega}$ denotes Young's Modulus of the direction $\boldsymbol{\omega}$. l_1, l_2 and l_3 are the directional cosines of $\boldsymbol{\omega}$. s_{11}, s_{13}, s_{33}, and s_{44} denote elastic compliance.

III. RESULTS AND DISCUSSION

As shown in Fig. 1, recent experiments show the solid-superionic and superionic-superionic phase transitions (ice X to ice XVIII) of ice at ~200 GPa with elaborating temperature suggesting the presence of SI ice in the interior of Uranus and Neptune [18]. Therefore, we constructed structures of ice X (bcc), and ice XVIII (fcc) in supercells with different cell parameters at 500–4500 K and 200 GPa. We determined the equilibrium volume and cell parameters at different temperatures by conducting a grid of NVT ensemble simulations over volumes and temperatures using a Nosé thermostat [35]. For each equilibrium structure at different temperatures, lattice parameters (Table I) were optimized to maintain the

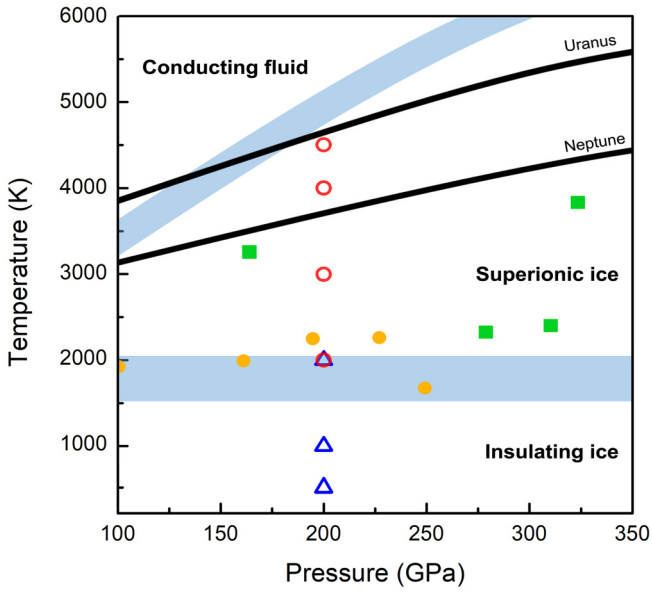

FIG. 1. The phase diagram of H_2O at high P-T. The blue zones are the boundaries of phase transition from ice X to ice XVIII, and to conducting fluid. The yellow solid circles and green solid squares represent stable P-T conditions for ice X and ice XVIII [18]. The blue open triangles and red circles represent the P-T conditions of our simulations for ice X and ice XVIII, respectively. The black-thick-solid curves show the thermal states in the interior of Uranus and Neptune.

hydrostatic stress under 200 GPa, and the calculated density-pressure relations at different temperatures are consistent with previous experiments [18,36] (Fig. S1).

The calculated three independent elastic constants (C_{11}, C_{12}, and C_{44}) of ice X and ice XVIII at different temperatures are shown in Fig. 2(a). The elastic constants of ice X decrease as the temperature increases from 500 to 1000 K, which is the normal behavior of a solid. Upon the superionic transition in ice X at 2000 K, we observed significant reductions in C_{11}, shear modulus (G), and shear wave velocity (V_S) [Fig. 2(b) and 2(c)]. Ice X transforms to ice XVIII at the temperature above 2000 K [18]. The transition leads to anisotropic elastic softening. The reduction ratios are 7.21%, 11.34%, and 29.86% for C_{11}, C_{12}, and C_{44}, respectively. The evolution of elastic constants above 2000 K in ice XVIII are quite anomalous. From 2000 to 3000 K, C_{11} and C_{12} increase slightly accompanied with the decreasing of density from 3.67 to 3.61 g cm^{-3}. Similar to the elastic constants, the moduli and sound velocities also show anisotropic evolution above 2000 K.

The ice X to ice XVIII phase transition at 2000 K leads to obvious decreases in both anisotropy factor ($A = \frac{2C_{44}}{C_{11}-C_{12}}$) and Poisson's ratio ($\nu = \frac{3B-G}{2(3B+G)}$) [Fig. 2(d)]. For temperatures above 2000 K, the A and ν generally increase with temperature. The detailed evolution of elastic anisotropy can be properly visualized using the three-dimensional (3D) directional dependence of the elastic anisotropy of Young's moduli (Fig. 3). Young's moduli are higher along the ⟨111⟩ directions compared to other directions, and the anisotropy is more pronounced in ice X than in ice XVIII.

The elastic constants and sound velocities in solid decrease with increasing temperature because of thermal expansion effects [33,37]. In SI ice, the density of ice XVIII does decrease from 3.67 to 3.61 g cm^{-3} when temperature increases from 2000 to 3000 K, but C_{11}, C_{12}, B, V_P, and V_Φ show slight increases (Table I). This behavior is quite unusual in solids and may be related with superionic protons. To understand this behavior, we calculated the proton diffusion coefficients and conductivities in SI ice (Fig. 4). For ice X, the proton diffusion coefficient increases by over 2 orders of magnitude to $\sim 10^{-6}$ cm^2 s^{-1} when the temperature is increased from 1000 to 2000 K indicating a solid-superionic phase transition. When the ice X to ice XVIII phase transition takes place at ~2000 K, the proton diffusion coefficient of ice XVIII is higher than that of ice X by over two orders of magnitude, and further increases above 10^{-3} cm^2 s^{-1} at 4000 K. The proton diffusion rate is much higher in ice XVIII than in ice X. The difference in proton diffusion behavior in the two phases can also be seen from the trajectories of H and O ions viewed along the [100] direction as shown in the insets of Fig. 4. Although the diffusion coefficients increase dramatically in ice X at 2000 K, the trajectory of protons still maintains a long-range periodic structure, and protons distribute about the symmetric sites of O-O. In this case, protons in ice X still behave like solids, and the elastic constants decrease

TABLE I. Calculated elastic constants, density, moduli, cell parameters, and velocities.

Phase	Ice X			Ice XVIII			
T (K)	500	1000	2000	2000	3000	4000	4500
P (GPa)	200.0	200.3	200.0	199.8	199.9	200.0	199.8
C_{11} (GPa)	922.8	893.2	794.9	737.6	759.1	700.4	670.1
C_{12} (GPa)	791.0	748.2	685.0	607.3	640.0	594.3	595.9
C_{44} (GPa)	471.8	453.3	430.0	301.6	288.7	225.3	268.6
ρ (g/cm^3)	3.72	3.70	3.65	3.67	3.61	3.55	3.52
V_Φ (km/s)	14.97	14.68	14.06	13.32	13.73	13.31	13.28
V_P (km/s)	17.44	17.21	16.43	15.40	15.68	15.00	14.98
V_S (km/s)	7.74	7.78	7.36	6.70	6.56	5.98	5.99
B (GPa)	834.93	796.53	721.70	650.73	679.70	629.67	620.63
G (GPa)	222.83	223.58	197.57	164.91	155.37	127.2	126.42
a (Å)	7.57	7.59	7.62	9.59	9.64	9.69	9.72

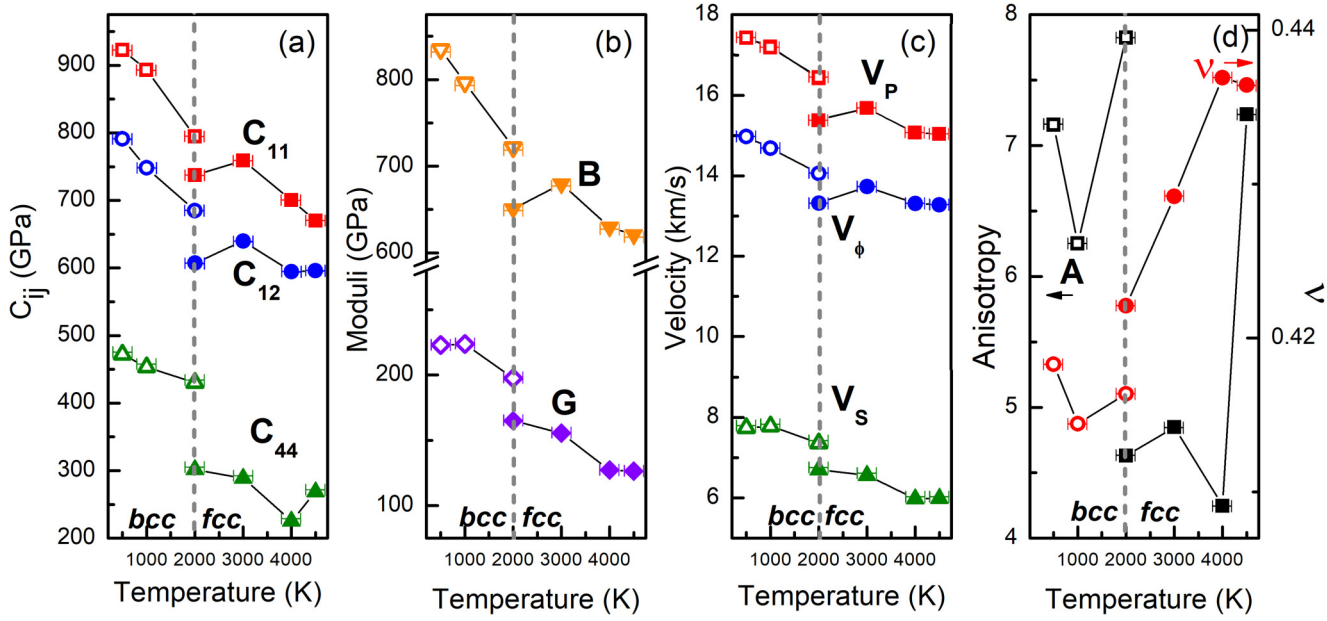

FIG. 2. Calculated elastic properties of ice X and ice XVIII at 200 GPa and 500–4500 K. The data of ice X and ice XVIII are labeled with open and solid symbols, respectively. (a) The elastic constants C_{11}, C_{12}, and C_{44} are represented by red squares, blue circles, and green triangles. (b) The bulk (B) and shear (G) moduli are displayed by orange triangles and purple squares. (c) The primary wave velocity (V_P), shear wave velocity (V_S), and bulk sound velocity (V_ϕ) are shown with red squares, green triangles, and blue circles, respectively. (d) The elastic anisotropy (A) and Poisson's ratio (ν) are shown with red circles and black squares, respectively.

with temperature. On the contrary, the diffusive protons in ice XVIII are highly disordered and behave similar to liquid flowing around the lattice. Hence, the ice X to ice XVIII phase transition leads to the solid-liquid transition of protons in the lattice. In general, there are two phase transitions in ice with increasing temperature. The first is the solid-superionic

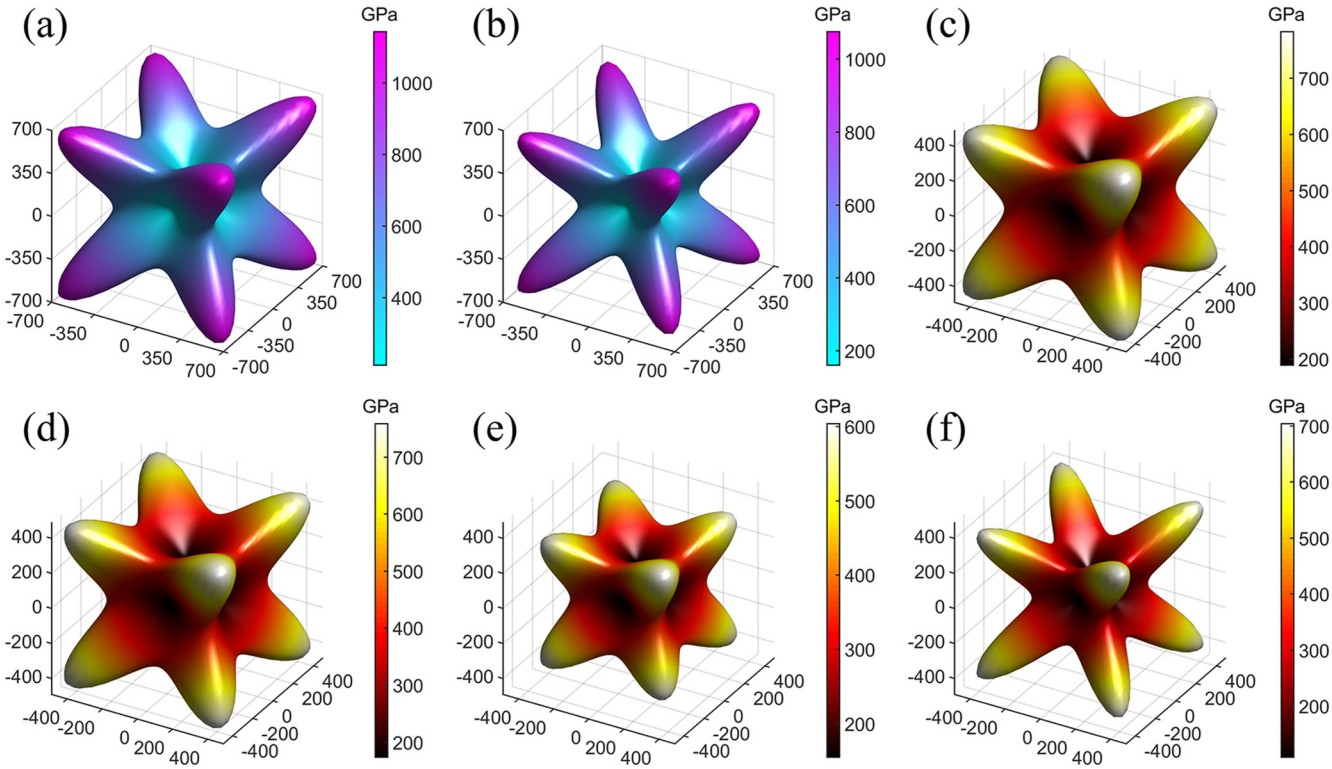

FIG. 3. 3D directional dependence of the elastic anisotropy of Young's modulus of ice X at (a) 1000 K, (b) 2000 K, and ice XVIII at (c) 2000 K, (d) 3000 K, (e) 4000 K, and (f) 4500 K.

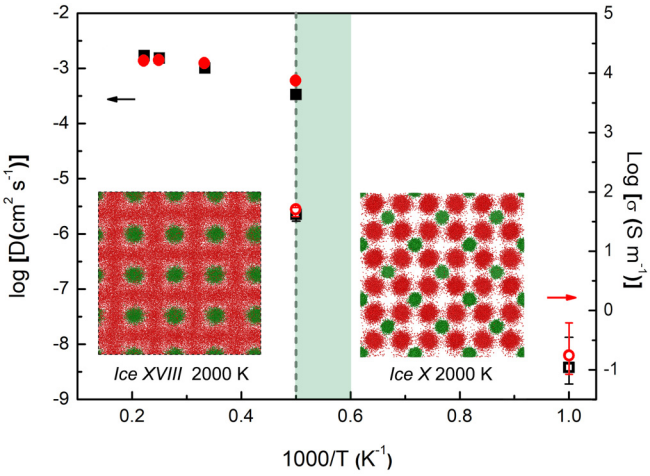

FIG. 4. The proton diffusion coefficients (black symbols) and conductivities (red symbols) in ice X and ice XVIII as the function of inverse temperature. The data for ice X and ice XVIII are displayed with open and solid symbols, respectively. The insets are the trajectories of H and O ions in ice X and ice XVIII at 2000 K. The red and green bullets represent H and O ions, respectively. The light green region indicates the solid-superionic transition temperature in ice X.

transition in ice X, in which protons become highly diffusive and dislocated. In the second transition from ice X to ice XVIII, protons change to disordered distribution with high diffusion coefficients (Figs. S8–S10).

We calculated the radial distribution function (RDF) of H-O to analyze the local structure change of the SI ice with increasing temperature (Fig. 5). Due to the high proton mobility, the RDF changes obviously with temperature and the phase transition from ice X to ice XVIII resulting in quite different H-O interaction. The change of the structure should has impact on the elastic properties. In ice X, the broadening of RDF peaks suggest more protons diffuse into interstitial sites with increasing temperature. The dislocated protons are responsible for the significant reductions in C_{11}, G, and V_S of SI ice X at 2000 K as the similar effect has been observed in the SI transition of Li_2O at ~1300 K [38]. The distribution of proton is more homogenous in ice XVIII with respective to H-O distance. The disordered protons in ice XVIII change their sites in the lattice and make the cell more flexible during deformation, which may reveal a weak H-O interaction inducing the observed elastic softening and reductions in sound velocities upon the ice X to ice XVIII phase transition. The RDF also indicates that the liquidlike superionic protons in ice XVIII still maintain a strong interaction with the periodic oxygen sublattice, and the extra entropy of liquidlike protons may enhance the structural strength with an increasing in diffusion rate, which provides an explanation on the elastic stiffening of ice XVIII from 2000 to 3000 K. Similar to ice XVIII, experimental studies show that sound velocities of water [39], liquid Fe-Ni-S [40,41] and many other liquid metals [42] present a positive correlation with temperature. Hence, the anomalous elastic stiffening of ice XVIII may also be a sign of liquidlike behavior of protons. Unlike the liquid phase, the stress of SI ice does not show obvious change during our simulation in a 1% strained model along the [100] direction for 100 ps (Fig. S3).

H_2O widely exists in planetary interior and plays an important role on the planetary evolution. SI ice are proposed to exist in the interior of Uranus and Neptune with influence on the origination of the nondipole magnetic fields [7,17–19]. Our study on the elastic properties of SI ice promotes our understanding on the interior of these planets and benefits the structure and dynamo modeling [20].

In Earth's interior, H_2O mainly exists in the form of hydroxyl in nominally anhydrous mineral and hydrous minerals. It is reported that hydrogen is able to diffuse in some minerals with high proton conductivities [43–46]. Recent theoretical prediction also suggests that hydrous minerals transfer to SI state under deep lower mantle conditions [47]. In this case, it is crucial to understand the effect of proton diffusion on elasticity of these hydrogen bearing minerals. In this study, the elastic properties and sound velocities of ice X and ice XVIII

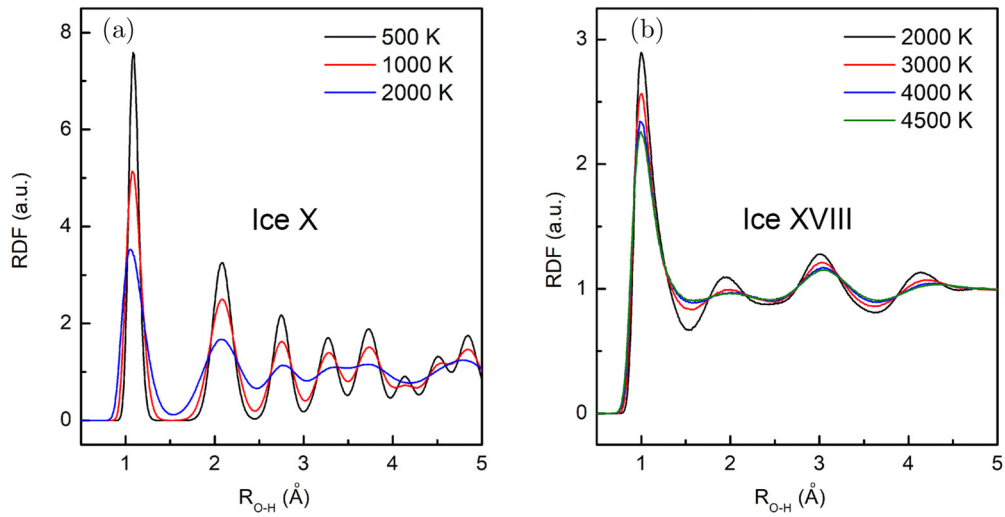

FIG. 5. Calculated radial distribution function (RDF) of H-O in ice X and ice XVIII at temperatures from 500 to 4500 K and pressure of 200 GPa.

are systematically studied, and proton diffusion has a significant influence on elastic properties. This result sheds lights on the possible different elastic properties of these minerals at high temperatures.

IV. CONCLUSIONS

Proton diffusion presents different behavior in SI ice X and ice XVIII. In ice X, the trajectory of the protons still maintains long-range order, and the elastic constants decrease with temperature like normal solid, while the disordered protons in ice XVIII result in obvious elastic softening during the ice X to ice XVIII phase transition. Unlike in a normal solid, extra entropy of liquidlike protons may lead to the elastic stiffening of ice XVIII from 2000 to 3000 K. This study shows that the liquidlike superionic protons have a profound effect on the elastic properties and sound velocity, which enhances our understanding of ice at high P-T, therefore helping us modeling the structure of the interior of giant exoplanets and inspiring the elasticity of superionic materials used in energy storage devices.

ACKNOWLEDGMENTS

This study was supported by the Strategic Priority Research Program (B) of the Chinese Academy of Sciences (XDB 18010401). We acknowledge the support of the National Natural Science Foundation of China (41774101) and the Youth Innovation Promotion Association of CAS (2020394). The manuscript was written with contributions from all authors. All authors have given approval to the final version of the manuscript.

[1] A. N. Dunaeva, D. V. Antsyshkin, and O. L. Kuskov, Sol. Syst. Res. **44**, 222 (2010).
[2] T. Bartels-Rausch, V. Bergeron, J. H. E. Cartwright, R. Escribano, J. L. Finney, H. Grothe, P. J. Gutiérrez, J. Haapala, W. F. Kuhs, J. B. C. Pettersson, S. D. Price, C. I. Sainz-Díaz, D. J. Stokes, G. Strazzulla, E. S. Thomson, H. Trinks, and N. Uras-Aytemiz, Rev. Mod. Phys. **84**, 885 (2012).
[3] A. F. Goncharov, V. V. Struzhkin, M. S. Somayazulu, R. J. Hemley, and H.-K. Mao, Science **273**, 218 (1996).
[4] M. Benoit, D. Marx, and M. Parrinello, Nature (London) **392**, 258 (1998).
[5] A. F. Goncharov, V. V. Struzhkin, H.-K. Mao, and R. J. Hemley, Phys. Rev. Lett. **83**, 1998 (1999).
[6] P. Demontis, R. LeSar, and M. L. Klein, Phys. Rev. Lett. **60**, 2284 (1988).
[7] C. Cavazzoni, G. L. Chiarotti, S. Scandolo, E. Tosatti, M. Bernasconi, and M. Parrinello, Science **283**, 44 (1999).
[8] N. Goldman, L. E. Fried, I. F. W. Kuo, and C. J. Mundy, Phys. Rev. Lett. **94**, 217801 (2005).
[9] T. R. Mattsson and M. P. Desjarlais, Phys. Rev. Lett. **97**, 017801 (2006).
[10] H. F. Wilson, M. L. Wong, and B. Militzer, Phys. Rev. Lett. **110**, 151102 (2013).
[11] J. Sun, B. K. Clark, S. Torquato, and R. Car, Nat. Commun. **6**, 8156 (2015).
[12] J.-A. Hernandez and R. Caracas, Phys. Rev. Lett. **117**, 135503 (2016).
[13] M. French, M. P. Desjarlais, and R. Redmer, Phys. Rev. E **93**, 022140 (2016).
[14] R. Chau, A. C. Mitchell, R. W. Minich, and W. J. Nellis, J. Chem. Phys. **114**, 1361 (2001).
[15] A. F Goncharov, N. Goldman, L. E. Fried, J. C. Crowhurst, I.-F. W. Kuo, C. J. Mundy, and J. M. Zaug, Phys. Rev. Lett. **94**, 125508 (2005).
[16] E. Sugimura, T. Komabayashi, K. Ohta, K. Hirose, Y. Ohishi, and L. S. Dubrovinsky, J. Chem. Phys. **137**, 194505 (2012).
[17] M. Millot, S. Hamel, J. R. Rygg, P. M. Celliers, G. W. Collins, F. Coppari, D. E. Fratanduono, R. Jeanloz, D. C. Swift, and J. H. Eggert, Nat. Phys. **14**, 297 (2018).
[18] M. Millot, F. Coppari, J. R. Rygg, A. C. Barrios, S. Hamel, D. C. Swift, and J. H. Eggert, Nature (London) **569**, 251 (2019).
[19] R. Redmer, T. R. Mattsson, N. Nettelmann, and M. French, Icarus **211**, 798 (2011).
[20] S. Stanley and J. Bloxham, Nature (London) **428**, 151 (2004).
[21] M. Ahart, M. Somayazulu, S. A. Gramsch, R. Boehler, H.-K. Mao, and R. J. Hemley, J Chem. Phys. **134**, 124517 (2011).
[22] J. Tsuchiya and T. Tsuchiya, J Chem. Phys. **146**, 014501 (2017).
[23] M. Kuriakose, S. Raetz, Q. M. Hu, S. M. Nikitin, N. Chigarev, V. Tournat, A. Bulou, A. Lomonosov, P. Djemia, V. E. Gusev, and A. Zerr, Phys. Rev. B **96**, 134122 (2017).
[24] B. Journaux, R. Caracas, P. Carrez, K. Gouriet, P. Cordier, and I. Daniel, Phys. Earth Planet. Inter. **236**, 10 (2014).
[25] X. He, Y. Zhu, and Y. Mo, Nat. Commun. **8**, 15893 (2017).
[26] P. Hohenberg and W. Kohn, Phys. Rev. **136**, B864 (1964).
[27] W. Kohn and L. J. Sham, Phys. Rev. **140**, A1133 (1965).
[28] L. Vočadlo, D. P. Dobson, and I. G. Wood, Earth Planet. Sci. Lett. **288**, 534 (2009).
[29] M. Mattesini, A. B. Belonoshko, E. Buforn, M. Ramirez, S. I. Simak, A. Udías, H. K. Mao, and R. Ahuja, Proc. Natl. Acad. Sci. USA **107**, 9507 (2010).
[30] B. Martorell, L. Vočadlo, J. Brodholt, and I. G. Wood, Science **342**, 466 (2013).
[31] G. Kresse and J. Fürthmuller, Phys. Rev. B **54**, 11169 (1996).
[32] P. E. Blöchl, Phys. Rev. B **50**, 17953 (1994).
[33] Z. Wu, J. F. Justo, and R. M. Wentzcovitch, Phys. Rev. Lett. **110**, 228501 (2013).
[34] C. Zener, *Elasticity and Anelasticity of Metals* (University of Chicago Press, Chicago, 1948).
[35] S. Nosé, J. Chem. Phys. **81**, 511 (1984).
[36] See Supplemental Material at http://link.aps.org/supplemental/10.1103/PhysRevB.102.104108 for density-pressure relationship, elastic properties calculations and structures of superionic ice.
[37] Y. P. Varshni, Phys. Rev. B **2**, 3952 (1970).
[38] S. Hull, T. W. D. Farley, W. Hayes, and M. T. Hutchings, J. Nucl. Mater. **160**, 125 (1988).
[39] J. M. Zaug, L. E. Fried, E. H. Abramson, D. W. Hansen, J. C. Crowhurst, and W. M. Howard, High Pressure Res. **23**, 229 (2003).
[40] P. M. Nasch, M. H. Manghnani, and R. A. Secco, Science **277**, 219 (1997).

[41] Z. Jing, Y. Wang, Y. Kono, T. Yu, T. Sakamaki, C. Park, M. L. Rivers, S. R. Sutton, and G. Shen, Earth Planet. Sci. Lett. **396**, 78 (2014).
[42] S. Blairs, Inter. Mater. Rev. **52**, 321 (2007).
[43] D. J. Wang, M. Mookherjee, Y. S. Xu, and S. Karato, Nature (London) **443**, 977 (2006).
[44] X. Huang, Y. Xu, and S. Karato, Nature (London) **434**, 746 (2005).
[45] L. Dai and S. Karato, Earth Planet. Sci. Lett. **408**, 79 (2014).
[46] X. Guo and T. Yoshino, Geophys. Res. Lett. **41**, 813 (2014).
[47] Y. He, D. Y. Kim, C. J. Pickard, R. J. Needs, Q. Hu, and H.-K. Mao, arXiv:1810.08766.